

Article

Evaluation of Bronopol and Disulfiram as Potential *Candidatus Liberibacter asiaticus* Inosine 5'-Monophosphate Dehydrogenase Inhibitors by Using Molecular Docking and Enzyme Kinetic

Jing Nan ¹ , Shaoran Zhang ², Ping Zhan ¹ and Ling Jiang ^{1,*}

¹ College of Horticulture and Forestry, Key Laboratory of Horticultural Plant Biology of Ministry of Education, Huazhong Agricultural University, Wuhan 430070, China; nanjing@webmail.hzau.edu.cn (J.N.); zhanping818@163.com (P.Z.)

² State Key Laboratory of Agricultural Microbiology, Huazhong Agricultural University, Wuhan 430070, China; zsr758991@163.com

* Correspondence: jiangling@mail.hzau.edu.cn

Received: 10 April 2020; Accepted: 11 May 2020; Published: 14 May 2020



Abstract: Citrus huanglongbing (HLB) is a destructive disease that causes significant damage to many citrus producing areas worldwide. To date, no strategy against this disease has been established. Inosine 5'-monophosphate dehydrogenase (IMPDH) plays crucial roles in the de novo synthesis of guanine nucleotides. This enzyme is used as a potential target to treat bacterial infection. In this study, the crystal structure of a deletion mutant of CLas IMPDH Δ 98-201 in the apo form was determined. Eight known bioactive compounds were used as ligands for molecular docking. The results showed that bronopol and disulfiram bound to CLas IMPDH Δ 98-201 with high affinity. These compounds were tested for their inhibition against CLas IMPDH Δ 98-201 activity. Bronopol and disulfiram showed high inhibition at nanomolar concentrations, and bronopol was found to be the most potent molecule ($K_i = 234$ nM). The K_i value of disulfiram was 616 nM. These results suggest that bronopol and disulfiram can be considered potential candidate agents for the development of CLas inhibitors.

Keywords: *Candidatus Liberibacter asiaticus*; Inosine 5'-monophosphate dehydrogenase; crystal; molecular docking; enzyme activity; antibacterial compound

1. Introduction

Huanglongbing (HLB) is one of the most destructive citrus diseases; it affects the citrus industry worldwide. HLB is a phloem-restricted, Gram-negative bacterium and caused by *Candidatus Liberibacter asiaticus* (CLas), *Candidatus Liberibacter africanus*, and *Candidatus Liberibacter americanus*. The pathogen is transmitted by the citrus psyllid [1]. CLas is highly virulent and distributed worldwide. HLB can infect all commercial varieties of cultivated citrus, and has caused enormous economic losses in the past [2]. Although some developments on CLas and plant-Liberibacter interaction have been achieved, no effective management method is presently available to control this disease once the trees are infected [3–9]. In September 2019, Ha and Beyenal from Washington State University were part of a research team that determined the process of culturing in a laboratory the bacteria that cause citrus greening. However, the culture technology of HLB has not been used in the development of drugs to control HLB [10]. Chemical control is considered to be an effective method to control citrus HLB. Controlling the transmit vector is a critical component which can slow down the spread, but it is not sufficient to eliminate this disease. Additional attempts have focused on the pathogen, and some broad-spectrum antimicrobials have been used against *Ca. Liberibacter* spp [11,12]. Streptomycin,

penicillin G, and oxytetracycline reduce the titer of CLAs in infected trees, but they also affect the native microbiota [13–15]. Compounds specifically targeting CLAs have also been confirmed [16–19]. However, to date, no agents have been used commercially to combat this disease in the field. Targeting small-molecule inhibitors of pathogenic proteins is a new concept to control HLB. This process is potentially valuable to identify a new target to treat HLB infection.

Purine metabolism is critical for the growth and virulence of many bacterial pathogens [20–23]. Inosine 5'-monophosphate dehydrogenase (IMPDH) is the first and rate-limiting step in guanine nucleotide biosynthesis, controlling the gateway to guanine nucleotides. IMPDH catalyzes the oxidation of inosine 5'-monophosphate to xanthosine 5'-monophosphate (XMP) with a concomitant reduction of NAD⁺ to NADH. Guanosine 5'-monophosphate synthetase (GMPS) subsequently converts XMP to guanosine 5'-monophosphate (GMP). Almost every organism, except *Giardia lamblia* and *Trichomonas vaginalis*, has the IMPDH/GMPS pathway [24,25]. Bacteria can also acquire guanine nucleotides through the salvage pathways. However, in microbial infection, rapid proliferation places the demand upon the guanine nucleotide that the purine salvage pathway be insufficient for bacteria survival. The inhibition of IMPDH results in the depletion of guanine nucleotides. In recent decade, numerous IMPDH inhibitors have been used as anticancer, antiviral, and immunosuppressive agents [26–28]. IMPDH is also a promising target for antibacterial drug discovery [29–32].

The crystal structure of IMPDH in bacteria such as *Tritrichomonas foetus*, *Bacillus anthracis*, and *Pseudomonas aeruginosa* exists as a tetramer with a D4 square planar symmetry [33–35]. A monomer consists of two domains, namely, the catalytic domain, which is an eight-fold β/α barrel, and a subdomain, including two tandem cystathione-synthetase motifs (CBS domain or Bateman domain), which protrudes from the corners of the homotetramer [36]. The function of the CBS domain remains unclear. Deletion of the CBS subdomain by mutagenesis has little or no effect on enzymatic activity, but improves stabilization and crystallization [37–39].

To date, over 100 crystal structures of IMPDH have been added to the Protein Data Bank (PDB). Information on the binding sites between the protein and substrate, cofactor, or inhibitors is revealed from these crystal structures. Although eukaryotic and prokaryotic IMPDHs have similar overall structures, their kinetic properties and sensitivities to inhibitors are significantly different [40]. Structural comparisons revealed that the IMP binding site is well defined and highly conserved. By contrast, among IMPDHs, the cofactor site is more diverse, and species-specific inhibitors targeting this site have been developed [41]. One of the earliest reports discovered pathogenic IMPDH inhibitors in a high-throughput screening of small molecules against *Cryptosporidium parvum* IMPDH (CpIMPDH) [42]. Significant success has been achieved in the development of inhibitors of bacterial IMPDH, such as benzimidazoles, benzoxazoles, indazoles, triazoles, isobenzofurans, arylurea derivatives, and indoles [43–57]. Although bacterial IMPDHs have high sequence similarities and many species have the IMSM motif, the structure–activity relationships of each inhibitor are different [39,43]. Accordingly, simple predictions regarding compounds targeting a specific IMPDH are not sufficient, and experimental validation is necessary.

In this study, a CLAs IMPDH variant without the CBS domain (CLAs IMPDH Δ 98-201) was designed. The recombinant CLAs IMPDH Δ 98-201 protein was expressed in the *Escherichia coli* system and purified using a Ni-NTA resin affinity chromatograph and high-resolution gel filtration column. The crystal structure of CLAs IMPDH Δ 98-201 was determined in the apo form. Repurposing drugs for a new target is increasingly used to find novel compounds. Eight known bioactive compounds were selected for molecular docking analysis, and the binding affinities were assessed. The inhibitions of these compounds against CLAs IMPDH Δ 98-201 activity were tested in vitro.

2. Results

2.1. Protein Purification of CLAs IMPDH Δ 98-201 and Crystallization Screening

To get the CBS deletion construct, 104 residues (98-201aa) were replaced with a G amino acid, and the catalytic residue Cys309 was completely conserved (Figure 1a). In the *E. coli* express system,

recombinant CLas IMPDH Δ 98-201 was soluble and stable. This protein was purified using a Ni-NTA resin affinity chromatograph and a high-resolution gel filtration column (Superdex 200), which showed a main peak (Figure 1b). CLas IMPDH Δ 98-201 consisted of 390 amino acids with a theoretical molecular mass of 41 kDa. CLas IMPDH Δ 98-201 appeared as a single band at approximately 40 kDa (Figure 1c).

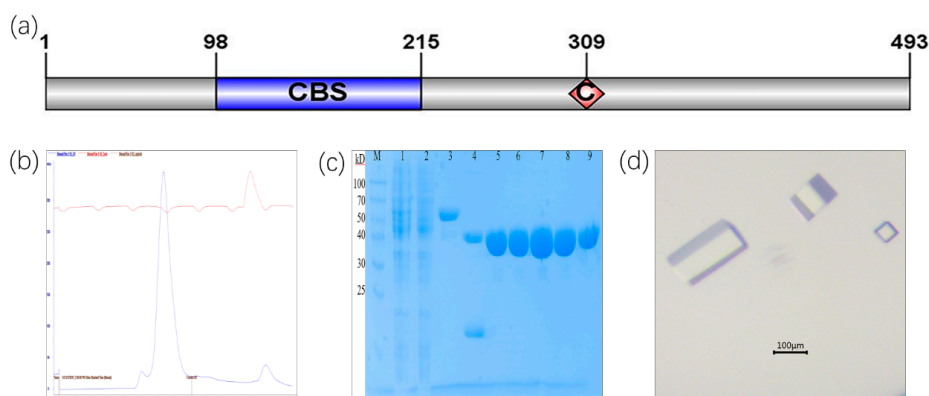


Figure 1. Size exclusion chromatogram and crystal of purified CLas IMPDH Δ 98-201. (a): Primary sequence of CLas IMPDH; (b): Size exclusion chromatogram of CLas IMPDH Δ 98-201; (c): SDS-PAGE of CLas IMPDH Δ 98-201. M: protein marker; 1: supernatant; 2: flow-through; 3: SUMO-CLas IMPDH Δ 98-201; 4: Ulp1 digestion; 5–9: protein of CLas IMPDH Δ 98-201 after size exclusion chromatogram; (d): crystal of CLas IMPDH Δ 98-201.

The initial crystallization conditions that were tested from Index, SaltRx, PEG/Ion Screen, Crystal Screen kits (Hampton Research, Aliso Viejo, CA, USA), and the Wizard kit (Emerald BioSystems, Bainbridge Island, WA, USA). After the initial screening, crystals formed under two conditions only. After further optimization, diffraction-quality crystals were obtained by mixing 1 μ L of protein solution at 8 mg/mL with 1 μ L of reservoir solution (consisting of 30% PEG400, 200 mM sodium chloride, and 100 mM HEPES, pH 7.0) at 20 $^{\circ}$ C. Long rectangular crystals of approximately 0.2 \times 0.1 \times 0.05 mm formed (Figure 1d).

2.2. Crystal Structure and Loop Refinement of CLas IMPDH Δ 98-201

Crystals of CLas IMPDH Δ 98-201 appeared after 3 days at 293 K. The resolution of the diffracting crystal was 2.55 \AA . Data collection and refinement parameters are summarized in Table 1.

Table 1. Data collection and refinement statistics.

	CLas IMPDH Δ 98-201
Beamline	SSRF BEAMLINE BL17U
wavelength (\AA)	0.9792
Detector	ADSC QUANTUM 315r
resolution range (\AA)	42.47–2.55
space group	C 1 2 1
unit cell parameters (\AA)	a = 143.13, b = 134.86, c = 85.62
no. of residues/protein	390
Monomer molecular weight (kDa)	41.0
phasing method	MR
search model	chains A of 4R7J
Refinement resolution range (\AA)	42.46–2.55

Table 1. Cont.

	CLas IMPDH Δ 98-201
no. of reflections	50928
σ cutoff	1.36
R _{work}	0.222
R _{free}	0.264
mean B factor (\AA^2)	69.3
data completeness (%)	98.2
redundancy	2.58
Ramachandran plot [most favored/outliers (%)]	95.2/0.5
PDB entry	6KCF

The structure of CLas IMPDH Δ 98-201 was determined through molecular replacement using IMPDH from *Campylobacter jejuni* (PDB entry 4R7J) as a template. Finally, the structure was refined to 2.55 \AA resolution by using the PHENIX software. This crystal protein existed as a homotetramer (Figure 2a), which is well conserved in other IMPDHs. The space group of CLas IMPDH Δ 98-201 was C121, and the unit-cell parameters for CLas IMPDH Δ 98-201 were $a = 143.13$, $b = 134.86$, and $c = 85.62$ \AA .

The structure of CLas IMPDH Δ 98-201 was very well defined, and the refinement parameters were $R_{\text{work}} = 22.2\%$ and $R_{\text{free}} = 26.5\%$. A comparison of the structures of CLas IMPDH Δ 98-201 and BaIMPDH Δ 95-200 (Figure 2b) showed that the structure of CLas IMPDH Δ 98-201 was highly similar to that of BaIMPDH Δ 95-200 in its apo form. The RMSD was 0.929 \AA .

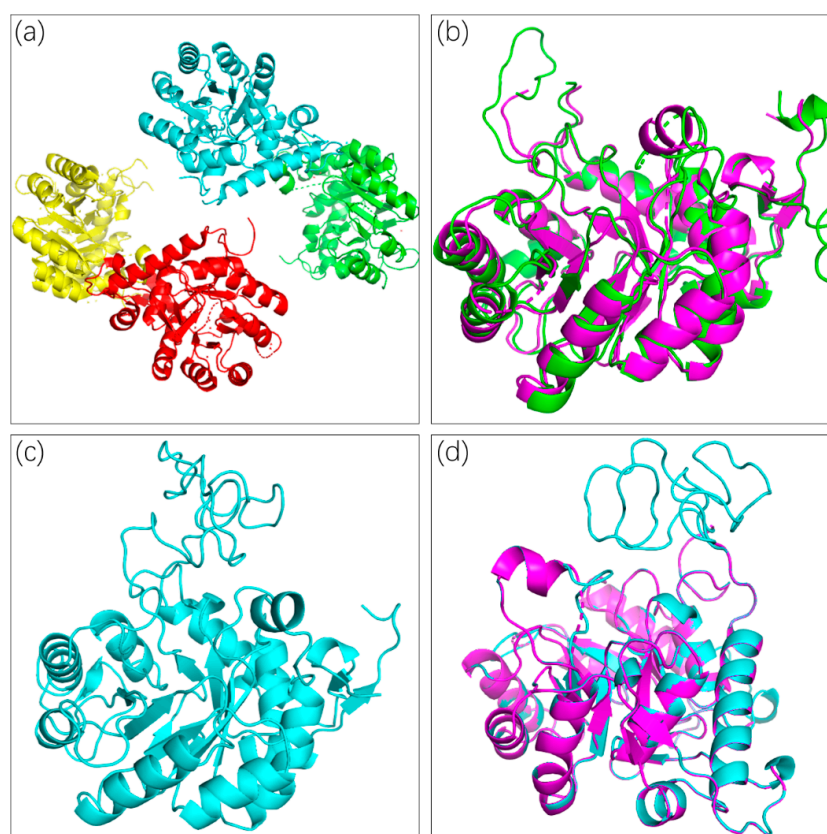


Figure 2. Crystal and Loop Refinement structure of the apo-form CLas IMPDH Δ 98-201. (a): Tetramer of CLas IMPDH Δ 98-201; (b): Superposed structures of CLas IMPDH Δ 98-201 (PDB entry: 6KCF, in magenta) and BaIMPDH Δ 95-200 (PDB entry: 4MJM, in green); (c): Loop refinement of CLas IMPDH Δ 98-201; (d): Superposed structures of CLas IMPDH Δ 98-201 (PDB entry: 6KCF, in green) and the refined structure (cyan).

The flap loop and a C-terminal loop are not visible in the electron density. Thus, the loop refinement of CLas IMPDH Δ 98-201 (PDB ID: 6KCF) was performed using Modeller 9.23 (Figure 2c). The nonterminal missing structure was refined (Figure 2d). Verification of the 3D results showed that 88.27% of the amino acid residues had an average 3D–1D score ≥ 0.2 (Figure S2). The Ramachandran plot analysis indicated that 82.4% of the residues were in the core region, 13.4% of the residues were in the allowed region, 2.9% of the residues were in the generously allowed region, and 1.3% of the residues were in the disallowed region (Figure S3).

2.3. Molecular Docking

The eight candidate compounds and the refined structure were selected to perform molecular docking. CDOCKER was used to perform a docking study of the selected molecule; the molecular docking binding affinities are shown in Table 2. Three molecules, namely, bronopol, mercaptopurine, and disulfiram, showed the $-CDOCKER_ENERGY \geq 10$. Because mercaptopurine is an analog of IMP, it was hypothesized that bronopol and disulfiram would exhibit the best inhibitory effect for CLas IMPDH. The pose with the lowest binding energy was recognized as the most stable conformation for further structural analysis.

Table 2. Detailed summary of the docking binding affinities (kcal/mol).

Name	Molecular Weight (g/mol)	-CDOCKER_ENERGY (kcal/mol)
Disulfiram	296.54	25.0346
Mercaptopurine	152.18	16.6785
Bronopol	199.99	11.1913
Ebselen	274.18	6.24157
Mycophenolic_acid	320.34	5.38177
Mizoribine	259.22	4.50734
Ribavirin	244.20	-5.62032
Mycophenolate_mofetil	433.50	-43.3176

The 3D and 2D structures of the CLas IMPDH Δ 98-201 with bronopol and disulfiram are displayed in Figure 3. Nine hydrogen bonds formed between bronopol and the residues ILE189, Gly190, Gly192, ASP228, Gly229, Gly230, Gly251, and Ser252 of CLas IMPDH Δ 98-201 (Figure 3a,b). Disulfiram formed two hydrogen bonds with CLas IMPDH Δ 98-201, namely, Ala41 and Ala42; four alkyl hydrophobic interaction with Met43, Pro190, and Met249; and one sulfur-x interaction with Met43 (Figure 3c,d). The 3D and 2D structures of the CLas IMPDH Δ 98-201 with the rest of molecules are displayed in Figure S4.

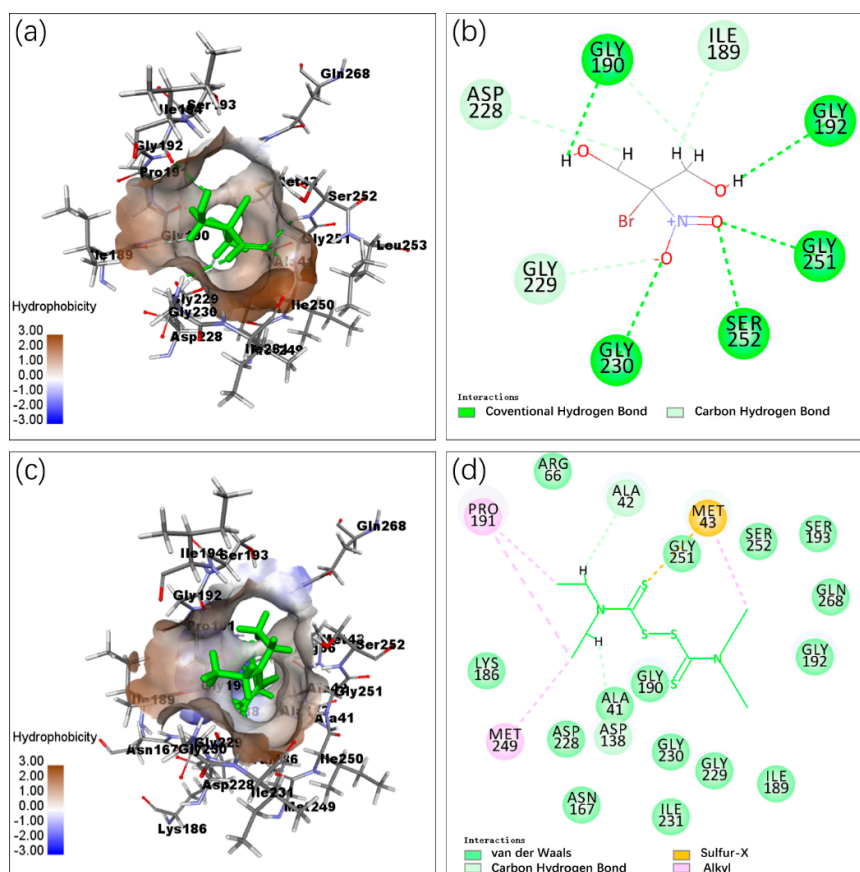


Figure 3. Molecular docking of CLas IMPDH Δ 98-201 and the molecules. (a): 3D details of CLas IMPDH Δ 98-201 and bronopol (green) interaction; (b): 2D details of CLas IMPDH Δ 98-201 and bronopol interaction; (c): 3D details of CLas IMPDH Δ 98-201 and disulfiram (green) interaction; (d): 2D details of CLas IMPDH Δ 98-201 and disulfiram interaction.

2.4. Kinetic Characterization of CLas IMPDH Δ 98-201

According to the standard assay conditions, the kinetic properties of CLas IMPDH Δ 98-201 were as follows: $K_{cat} = 7.2 \pm 0.2 \text{ s}^{-1}$; $K_M^{IMP} = 181 \pm 19 \text{ }\mu\text{M}$ (Figure 4a); and $K_M^{NAD^+} = 318 \pm 24 \text{ }\mu\text{M}$ (Figure 4b). Similar to other IMPDHs, substrate inhibition was also observed at high NAD^+ levels, $K_{ii}^{NAD^+} = 7.3 \pm 1.1 \text{ mM}$.

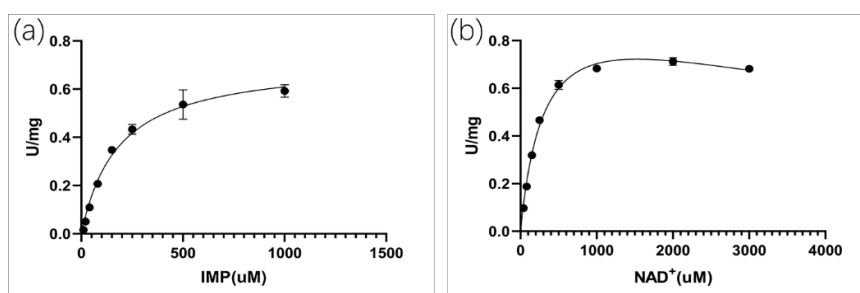


Figure 4. Enzyme activity of CLas IMPDH Δ 98-201. (a): Varying concentrations of IMP at a fixed concentration of NAD^+ (2 mM); (b): Varying concentrations of NAD^+ at a fixed concentration of IMP (1 mM).

The steady-state parameters from other bacterial species are listed in Table S2. All IMPDHs had similar K_m values for the substrate, but for CLas IMPDH Δ 98-201, K_M^{IMP} was the largest, and $K_M^{NAD^+}$ was the smallest. These results indicate that CLas IMPDH Δ 98-201 bound to IMP with the lowest affinity, but was the highest affinity binding NAD^+ among the tested IMPDHs. The K_{cat} value may be

due to the fact that the results described here were measured at 30 °C, whereas the other IMPDHs were measured at the lower temperature of 25 °C.

2.5. Inhibitory Assay against CLas IMPDH Δ 98-201 Enzyme Activity

Extending the measurement time, no exponential enzyme decay against CLas IMPDH Δ 98-201 was observed. Hence, the inhibition of bronopol, disulfiram, and ebselen was treated as a reversible mode (Figure S5). As shown in Figure S6a, the V_{max} was found to be reduced with an increase in the inhibitor concentration, suggesting that bronopol inhibited CLas IMPDH Δ 98-201 in a noncompetitive manner against IMP. Disulfiram also inhibited CLas IMPDH in a noncompetitive manner against IMP, where regression lines meet on the X-axis (Figure S6b). The various types of inhibition by other small molecule inhibitors are summarized in Figure S6.

To study the mechanism of enzyme inhibition, the inhibition constant K_i with respect to the IMP substrates was measured at a fixed NAD^+ concentration. The K_i values of these eight compounds are summarized in Table 3.

Table 3. Inhibition of CLas IMPDH Δ 98-201 by eight inhibitors.

Inhibitor	IMP K_i (μ M)
Bronopol	0.23 \pm 0.01
Disulfiram	0.62 \pm 0.04
Ebselen	4.13 \pm 0.19
Mycophenolic acid	2.43 \pm 0.10
Mercaptopurine	165 \pm 9.89
Mycophenolate mofetil	24.42 \pm 1.65
Mizoribine	307.7
Ribavirin	>3500

All values ranged from 0.234 μ M to 3500 μ M. Although the percentage of DMSO and the high concentration of the compound affected the stability of the target protein, the values for mizoribine and ribavirin may have been inaccurate (Figure S7c,f). Ribavirin is a guanosine analog with broad-spectrum activity against RNA virus [58], and has almost no effect on the CLas IMPDH Δ 98-201 enzyme activity. Mizoribine is an imidazole nucleoside which is used as an immunosuppressive agent [59]. Mizoribine was a potent inhibitor of IMPDHs, with $K_i = 307.7 \mu$ M for CLas IMPDH Δ 98-210, whereas the K_i value of *E. coli* IMPDH was 0.5 μ M. Mercaptopurine yielded uncompetitive inhibition with $K_i = 165 \mu$ M (Figure S7b). Mycophenolic acid was shown to be a potent inhibitor of mammalian IMPDHs with $K_i = 2.43 \mu$ M (Figure S7d). Mycophenolate mofetil is a prodrug of mycophenolic acid [60], yielding $K_i = 24.42 \mu$ M (Figure S7e). Three compounds, namely, disulfiram, bronopol, and ebselen, have been repurposed as IMPDH inhibitors [61]. Bronopol had the best inhibitory effect with $K_i = 234$ nM (Figure 5a). The K_i value of disulfiram was 616 nM (Figure 5b). The K_i values of ebselen was 4.13 μ M (Figure S7a).

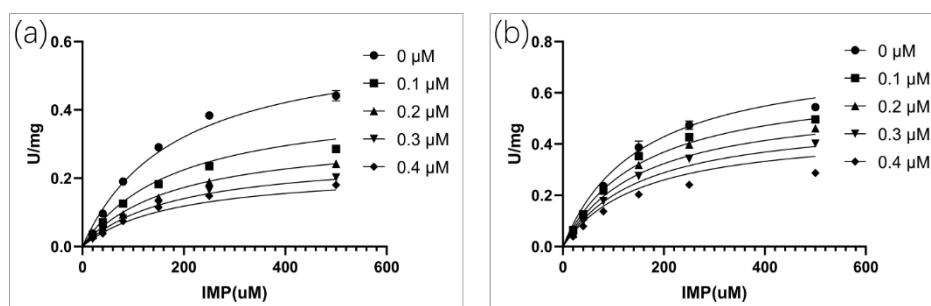


Figure 5. Inhibition kinetics at different concentrations of compounds by varying the IMP concentrations at a fixed NAD^+ concentration. (a): Bronopol; (b): Disulfiram.

3. Discussion

CLas causes HLB and affects citrus. Although HLB has become a global problem, no effective HLB management strategy is available [11]. IMPDH is a validated target for the design of potent antibacterial agents, and the inhibition of this enzyme depletes cellular guanine nucleotides [36]. The development of inhibitors against bacterial IMPDHs has attracted increasing attention [62]. This study focused on the development of CLas IMPDH inhibitors. The first structure of CLas IMPDH Δ 98-201 was determined. On the basis of its crystal structure, the refined structure was constructed, and molecular docking was performed to predict the binding energy. Then, we used an inhibition assay against CLas IMPDH Δ 98-201 to validate the molecular docking predictions.

3.1. Purification and Crystallization of CLas IMPDH Δ 98-201

To overcome the instability of CLas IMPDH, CLas IMPDH mutation was designed and purified. In the solution, recombinant CLas IMPDH Δ 98-201 was more stable than the wild type. MtbIMPDH2 without the CBS domain displayed higher solubility [51]. The steady-state kinetics parameters of CLas IMPDH Δ 98-201 were similar to those of other IMPDHs (Table S2), suggesting that deleting the CBS domain would not affect the CLas IMPDH Δ 98-201 catalytic properties [7]. Crystals of the apo form of CLas IMPDH Δ 98-201 were obtained in 100 mM HEPES (pH 7.5) and 200 mM NaCl, with 30% (w/v) PEG 4000 as the precipitant. The RMSD of CLas IMPDH Δ 98-201 and BaIMPDH Δ 95-200 was 0.929 Å.

3.2. Docking Interaction Analysis of CLas IMPDH Δ 98-201 with Molecules

To find inhibitors of CLas IMPDH Δ 98-201, molecular docking was performed using Discovery Studio 2018. The docking scores of bronopol and disulfiram binding to CLas IMPDH Δ 98-201 were -11.19 and -25.03 kcal/mol, respectively. Bronopol was stabilized by nine hydrogen bond interactions with residues ILE189, Gly190, Gly192, ASP228, Gly229, Gly230, Gly251, and Ser252. Additionally, disulfiram was stabilized by hydrophobic and sulfur-x interactions. Given that a flap loop and a C-terminal loop were not visible in the apo form structure of CLas IMPDH Δ 98-201, the nonterminal missing structure of CLas IMPDH Δ 98-201 was refined by Modeller. The Ramachandran plot and Verify 3D analysis suggested that the refined CLas IMPDH Δ 98-201 structure was reliable. Bacterial IMPDHs were similar in sequence and structure (Figure S1). Homology modeling and in silico docking were performed to study the structure–activity relationship of indole derivatives against *Helicobacter pylori* IMPDH [63]. The crystal structure of IMPDH from *Cricetulus griseus* was prepared by using Discovery Studio 2.5 to build a pharmacophore model of IMPDH inhibitors and for the in silico docking analysis [64]. These studies supported the feasibility of molecular docking.

3.3. Inhibitory Assay against CLas IMPDH Δ 98-201 Activity

To explore the inhibition of the eight compounds, an inhibitory assay against CLas IMPDH Δ 98-201 activity was measured by monitoring the production of NADH. The inhibitions of BaIMPDH Δ 92-220, CjIMPDH Δ 92-195, and ClpIMPDH Δ 89-215 to a given compound showed significant differences, although the same residues interacted with the inhibitor [7]. A previous study found that a single residue showed mycophenolic acid resistance, although the binding sites were identical [65]. The kinetic mechanism was controlled for the mycophenolic acid resistance of *Pb*IMPDH-A and *Pb*IMPDH-B [66]. These studies showed that virtual screening by simple prediction is fast and low cost, although experimental verification is needed. Many other compounds against HLB have been reported. Five compounds, namely, C16, C17, C18, C19, and C20, were identified against CLas SecA, with IC₅₀ values of 0.25, 0.92, 0.48, 0.64, and 0.44 μ M, respectively [16]. ZINC05491830 is one of the most potent inhibitors of CLas Esbp, with an IC₅₀ value of 2.59 μ M [19]. ChemDiv C549-0604 is an inhibitors of CLas VisNR, with an IC₅₀ value of 0.7 μ M [18]. The inhibition assay suggested that the K_i values of bronopol and disulfiram were 234 and 616 nM, respectively. The inhibition of CLas IMPDH Δ 98-201

suggested that bronopol and disulfiram, unlike the aforementioned other compounds, could be used as CLas IMPDH Δ 98-201 inhibitors against other CLas genes.

4. Materials and Methods

4.1. Cloning and Mutant Construction of CLas IMPDH Gene

The coding sequence of IMPDH was amplified by PCR from the chromosomal DNA of CLas (strain psy62). The PCR product was cloned into the pET28at-plus expression vector.

The CBS domain deletion mutant (CLas IMPDH Δ 98-201) was constructed via splicing overlapping extension polymerase chain reaction (PCR). The Δ S construct involved the deletion of 104 residues from M98 to T201. The CLas IMPDH gene in vector pET28at-plus was used as a template. The F1 and R1 primers were applied to amplify a region of CLas IMPDH ranging from residue M1 to residue M98. The F2 and R2 primers were used to amplify a region of CLas IMPDH ranging from residue T201 to residue I493. Codons for residues M98–T201 were replaced with codons for G. I1 and I2 were used as templates. PCR was performed to amplify the CLas IMPDH CBS domain deletion mutant gene by using the F1 and R2 primers. The CLas IMPDH Δ 98-201 gene was digested by *Bam* HI and *Xho* I and inserted into a pET28a-SUMO vector. Then, pET28a-SUMO-CLas IMPDH Δ 98-201 was transformed into *E. coli* BL21(DE3) cells.

4.2. Protein Purification and Crystallization of CLas IMPDH Δ 98-201

Cells carrying pET28a-SUMO-CLas IMPDH Δ 98-201 plasmid were cultured in LB media supplemented with 50 μ g/mL of kanamycin at 37 °C. The culture was induced by adding 0.3 mM of isopropyl- β -D-thiogalactopyranoside when its OD₆₀₀ reached 0.8–1.0. After 20 h of incubation at 16 °C, the cells were harvested by centrifugation at 6000 rpm for 6 min at 4 °C, resuspended in lysis buffer [20 mM Tris-HCl (pH 8.0), 500 mM KCl, 40 mM imidazole, 1 mM PMSF, and 10% glycerol], and then sonicated. The lysate was clarified by centrifugation at 16,000 rpm for 50 min at 4 °C. Clarified lysate was subsequently purified on a Ni-NTA agarose column, and the protein was eluted with the same buffer containing 500 mM imidazole. The SUMO tag was subsequently removed with the Ulp1 protease at 16 °C for 1 h. The target protein was additionally purified using a Ni affinity chromatograph to remove the released tag and uncut protein, followed by a size exclusion chromatography step on a SuperdexTM 200 (GE Healthcare) column equilibrated with buffer [20 mM Tris-HCl (pH 8.0), 100 mM KCl, and 10% glycerol]. All proteins were purified according to this protocol.

Crystallization screening was set up using the sitting drop vapor diffusion method in 96-well plates. Crystals of the protein appeared after 3 days at 293 K. The best crystals of CLas IMPDH Δ 98-201 were obtained by mixing 1 μ L of protein solution at 8 mg/mL with 1 μ L of reservoir solution consisting of 30% (v/v) PEG 400, 100 mM HEPES (pH 7.5), and 200 mM sodium chloride.

4.3. Data Collection and Processing

Crystals were mounted on nylon loops and flash-cooled in liquid nitrogen. Diffraction data were collected at 100 K by using the Q315r CCD detector at the BL17U beamline of the Shanghai Synchrotron Radiation Facility. Single wavelength data at 0.9792 Å were obtained, and all data were processed and scaled with HKL3000 [67]. The structure of the CLas IMPDH Δ 98-201 was solved by molecular replacement using PHENIX [68]. The refined model and structure factors were deposited in the PDB.

4.4. Loop Refinement and Molecular Docking

The 3D structure of CLas IMPDH Δ 98-201 was used for refinement. The Modeller program was used to refine the nonterminal missing structure [69]. This refined structure consisted of 358 amino acids (CLas IMPDH 12-98 and 202-472). The PROCHECK validation server was used to check the quality of the refined model [70]. This structure was also validated by Verify 3D [71].

Molecular docking was performed using CDOCKER, a frequently applied module of Discovery Studio 2018. CDOCKER employs a CHARMM force field to calculate the binding free energy of the ligand to the receptor [72]. The eight filtered molecules used for docking were bronopol, ebselen, mercaptopurine, mizoribine, mycophenolate_mofetil, mycophenolic acid, ribavirin, and disulfiram. In the docking experiment, the refined structure of CLas IMPDH Δ 98-201 was used as the receptor; the docking parameters are listed in Table S1. The best pose of each molecular binding with a refined structure was estimated according to the binding energy. Interactions between the compound and protein, such as van der Waals force, hydrogen bond, electrostatic, hydrophobic, and halogen, were analyzed.

4.5. Steady-State Kinetics

Standard enzyme activity assay was performed in an assay buffer (50 mM Tris-HCl, 100 mM KCl, 1 mM DTT, pH 8.0) and a final CLas IMPDH Δ 98-201 enzyme concentration of 100 nM at 30 °C. The production of NADH was monitored by the increase in absorbance at 340 nm ($\epsilon = 6.22 \text{ mM}^{-1} \times 0007 \text{ cm}^{-1}$). Apparent steady-state kinetic parameters were evaluated at varying concentrations of IMP (0.005–1 mM) and a fixed saturating concentration of NAD⁺ (3 mM), or at varying concentrations of NAD⁺ (0.005–5 mM) and a fixed saturation level of IMP (1 mM). Assays were performed in duplicate. The IMPDH enzymes displayed strong substrate inhibition with respect to NAD⁺ under the standard assay conditions. The method described by Kerr et al. was used to determine the kinetic constants [73].

4.6. Inhibition Assay against IMPDH Δ 98-201 of CLas

The eight molecules that were purchased were screened in vitro. The assay was performed in a 200 μ L final volume in a 96-well plate with a reaction buffer consisting of 50 mM Tris-HCl (pH 8.0), 100 mM KCl, and 1 mM dithiothreitol. Assays were performed using 100 nM CLas IMPDH Δ 98-201 in the presence or absence of test compounds. The assay was allowed to proceed at 30 °C for 60 min.

The value of K_i for eight molecules was determined at a fixed saturation concentration of NAD⁺ (1 mM), different concentrations of IMP (0.02, 0.04, 0.08, 0.15, 0.25, and 0.5 mM), and in the presence of increasing concentrations of inhibitor. The concentrations of bronopol and disulfiram were 0.1, 0.2, 0.3, 0.4 μ M. The concentration of ebselen was 1, 2, 3 and 4 μ M. The concentration of mycophenolic acid was 1, 2, 4 and 8 μ M. The concentration of mycophenolate mofetil ranged from 5 to 20 μ M. The concentration of mercaptopurine ranged from 50 to 200 μ M. The concentration of mizoribine was 500 and 750 μ M. The concentration of ribavirin was 500 and 800 μ M. Each determination of K_i was derived from duplicate measurements.

To determine the K_i values, the initial rate data versus substrate concentration at different inhibitor concentrations was fitted using Prism software (GraphPad) to equations for competitive, noncompetitive, or uncompetitive inhibition.

5. Conclusions

In conclusion, bronopol and disulfiram were confirmed as CLas IMPDH inhibitors. These results indicate that these compounds could be used as the lead scaffold to further design and develop potent CLas IMPDH inhibitors. However, the effect of compounds with activity against CLas was not tested. In future studies, we will focus on the effect of compounds in the treatment of HLB diseases. The apo form structure of CLas IMPDH Δ 98-201 was solved, providing a means to study the complex structure of cocrystallization with inhibitors. The binding information may be helpful for the further development of antimicrobial compounds against CLas.

Supplementary Materials: The following are available online.

Author Contributions: L.J. contributed to the project conceptualization; J.N. conducted the experiments; S.Z. analyzed the diffraction data and solved the structure; P.Z. contributed to experiment preparation. All authors have read and agreed to the published version of the manuscript.

Funding: This research was funded by National Natural Science Foundation of China (No. 31872064 and 31572099) and National key research and development plan (2018YFD0201500).

Acknowledgments: We thank the staff of the BL17U1 beamline of the NCPSS at the Shanghai Synchrotron Radiation Facility for assistance during data collection. We thank Ping Yin and Guiqing Peng from Huazhong Agricultural University for help in preparing crystal. We would be grateful to technical assistance from State Key Laboratory of Agricultural Microbiology Core Facility, Huazhong Agricultural University.

Conflicts of Interest: The authors declare no conflict of interest.

References

1. Bove, J.M. Huanglongbing: A destructive, newly-emerging, century-old disease of citrus. *J. Plant Pathol.* **2006**, *88*, 7–37.
2. Wang, N.; Pierson, E.A.; Setubal, J.C.; Xu, J.; Levy, J.G.; Zhang, Y.; Li, J.; Rangel, L.T.; Martins, J., Jr. The *Candidatus Liberibacter*-Host Interface: Insights into Pathogenesis Mechanisms and Disease Control. *Annu. Rev. Phytopathol.* **2017**, *55*, 451–482. [[CrossRef](#)]
3. Selvaraj, V.; Maheshwari, Y.; Hajeri, S.; Chen, J.; McCollum, T.G.; Yokomi, R. Development of a duplex droplet digital PCR assay for absolute quantitative detection of “*Candidatus Liberibacter asiaticus*”. *PLoS ONE* **2018**, *13*, e0197184. [[CrossRef](#)] [[PubMed](#)]
4. Jain, M.; Munoz-Bodnar, A.; Zhang, S.; Gabriel, D.W. A Secreted ‘*Candidatus Liberibacter asiaticus*’ Peroxiredoxin Simultaneously Suppresses Both Localized and Systemic Innate Immune Responses In Planta. *Mol. Plant Microbe Interact. MPMI* **2018**, *31*, 1312–1322. [[CrossRef](#)] [[PubMed](#)]
5. Clark, K.; Franco, J.Y.; Schwizer, S.; Pang, Z.; Hawara, E.; Liebrand, T.W.H.; Pagliaccia, D.; Zeng, L.; Gurung, F.B.; Wang, P.; et al. An effector from the Huanglongbing-associated pathogen targets citrus proteases. *Nat. Commun.* **2018**, *9*, 1718. [[CrossRef](#)] [[PubMed](#)]
6. Jain, M.; Munoz-Bodnar, A.; Gabriel, D.W. ‘*Candidatus Liberibacter asiaticus*’ peroxiredoxin (LasBCP) suppresses oxylipin-mediated defense signaling in citrus. *J. Plant Physiol.* **2019**, *236*, 61–65. [[CrossRef](#)]
7. Zhang, C.; Wang, X.; Liu, X.; Fan, Y.; Zhang, Y.; Zhou, X.; Li, W. A Novel ‘*Candidatus Liberibacter asiaticus*’-Encoded Sec-Dependent Secretory Protein Suppresses Programmed Cell Death in *Nicotiana benthamiana*. *Int. J. Mol. Sci.* **2019**, *20*, 5802. [[CrossRef](#)]
8. Shi, Q.; Pitino, M.; Zhang, S.; Krystel, J.; Cano, L.M.; Shatters, R.G., Jr.; Hall, D.G.; Stover, E. Temporal and spatial detection of *Candidatus Liberibacter asiaticus* putative effector transcripts during interaction with Huanglongbing-susceptible, -tolerant, and -resistant citrus hosts. *BMC Plant Biol.* **2019**, *19*, 122. [[CrossRef](#)]
9. Ramadugu, C.; Keremane, M.L.; Halbert, S.E.; Duan, Y.P.; Roose, M.L.; Stover, E.; Lee, R.F. Long-Term Field Evaluation Reveals Huanglongbing Resistance in Citrus Relatives. *Plant Dis.* **2016**, *100*, 1858–1869. [[CrossRef](#)]
10. Phuc, T.H.; He, R.F.; Nabil, K.; Judith, K.B.; Anders, O.; David, R.G.; Haluk, B. Host-free biofilm culture of “*Candidatus Liberibacter asiaticus*”, the bacterium associated with Huanglongbing. *Biofilm* **2019**, *1*, 100005.
11. Wang, N. The Citrus Huanglongbing Crisis and Potential Solutions. *Mol. Plant* **2019**, *12*, 607–609. [[CrossRef](#)]
12. Blaustein, R.A.; Lorca, G.L.; Teplitski, M. Challenges for Managing *Candidatus Liberibacter* spp. (Huanglongbing Disease Pathogen): Current Control Measures and Future Directions. *Phytopathology* **2018**, *108*, 424–435. [[CrossRef](#)] [[PubMed](#)]
13. Zhang, M.; Powell, C.A.; Zhou, L.; He, Z.; Stover, E.; Duan, Y. Chemical compounds effective against the citrus Huanglongbing bacterium ‘*Candidatus Liberibacter asiaticus*’ in planta. *Phytopathology* **2011**, *101*, 1097–1103. [[CrossRef](#)] [[PubMed](#)]
14. Shin, K.; Ascunce, M.S.; Narouei-Khandan, H.A.; Sun, X.A.; Jones, D.; Kolawole, O.O.; Goss, E.M.; van Bruggen, A.H.C. Effects and side effects of penicillin injection in huanglongbing affected grapefruit trees. *Crop Prot.* **2016**, *90*, 106–116. [[CrossRef](#)]
15. Hu, J.; Wang, N. Evaluation of the Spatiotemporal Dynamics of Oxytetracycline and Its Control Effect against Citrus Huanglongbing via Trunk Injection. *Phytopathology* **2016**, *106*, 1495–1503. [[CrossRef](#)]
16. Akula, N.; Trivedi, P.; Han, F.Q.; Wang, N. Identification of small molecule inhibitors against SecA of *Candidatus Liberibacter asiaticus* by structure based design. *Eur. J. Med. Chem.* **2012**, *54*, 919–924. [[CrossRef](#)]
17. Gardner, C.L.; Pagliai, F.A.; Pan, L.; Bojilova, L.; Torino, M.I.; Lorca, G.L.; Gonzalez, C.F. Drug Repurposing: Tolfenamic Acid Inactivates PrbP, a Transcriptional Accessory Protein in *Liberibacter asiaticus*. *Front. Microbiol.* **2016**, *7*, 1630. [[CrossRef](#)]

18. Barnett, M.J.; Solow-Cordero, D.E.; Long, S.R. A high-throughput system to identify inhibitors of *Candidatus Liberibacter asiaticus* transcription regulators. *Proc. Natl. Acad. Sci. USA* **2019**, *116*, 18009–18014. [[CrossRef](#)]
19. Saini, G.; Dalal, V.; Savita, B.K.; Sharma, N.; Kumar, P.; Sharma, A.K. Molecular docking and dynamic approach to virtual screen inhibitors against Esbp of *Candidatus Liberibacter asiaticus*. *J. Mol. Graph. Model.* **2019**, *92*, 329–340. [[CrossRef](#)]
20. Jewett, M.W.; Lawrence, K.A.; Bestor, A.; Byram, R.; Gherardini, F.; Rosa, P.A. GuaA and GuaB are essential for *Borrelia burgdorferi* survival in the tick-mouse infection cycle. *J. Bacteriol.* **2009**, *191*, 6231–6241. [[CrossRef](#)]
21. Yoshioka, S.; Newell, P.D. Disruption of de novo purine biosynthesis in *Pseudomonas fluorescens* Pf0-1 leads to reduced biofilm formation and a reduction in cell size of surface-attached but not planktonic cells. *PeerJ* **2016**, *4*, e1543. [[CrossRef](#)] [[PubMed](#)]
22. Boitz, J.M.; Jardim, A.; Ullman, B. GMP reductase and genetic uncoupling of adenylate and guanylate metabolism in *Leishmania donovani* parasites. *Mol. Biochem. Parasitol.* **2016**, *208*, 74–83. [[CrossRef](#)] [[PubMed](#)]
23. Kofoed, E.M.; Yan, D.; Katakam, A.K.; Reichelt, M.; Lin, B.; Kim, J.; Park, S.; Date, S.V.; Monk, I.R.; Xu, M.; et al. De Novo Guanine Biosynthesis but Not the Riboswitch-Regulated Purine Salvage Pathway Is Required for *Staphylococcus aureus* Infection in vivo. *J. Bacteriol.* **2016**, *198*, 2001–2015. [[CrossRef](#)] [[PubMed](#)]
24. Morrison, H.G.; McArthur, A.G.; Gillin, F.D.; Aley, S.B.; Adam, R.D.; Olsen, G.J.; Best, A.A.; Cande, W.Z.; Chen, F.; Cipriano, M.J.; et al. Genomic minimalism in the early diverging intestinal parasite *Giardia lamblia*. *Science* **2007**, *317*, 1921–1926. [[CrossRef](#)]
25. Carlton, J.M.; Hirt, R.P.; Silva, J.C.; Delcher, A.L.; Schatz, M.; Zhao, Q.; Wortman, J.R.; Bidwell, S.L.; Alsmark, U.C.; Besteiro, S.; et al. Draft genome sequence of the sexually transmitted pathogen *Trichomonas vaginalis*. *Science* **2007**, *315*, 207–212. [[CrossRef](#)] [[PubMed](#)]
26. Allison, A.C.; Almquist, S.J.; Muller, C.D.; Eugui, E.M. In vitro immunosuppressive effects of mycophenolic acid and an ester pro-drug, RS-61443. *Transplant. Proc.* **1991**, *23*, 10–14.
27. Robins, R.K.; Revankar, G.R.; McKernan, P.A.; Murray, B.K.; Kirsi, J.J.; North, J.A. The importance of IMP dehydrogenase inhibition in the broad spectrum antiviral activity of ribavirin and selenazofurin. *Adv. Enzyme Regul.* **1985**, *24*, 29–43. [[CrossRef](#)]
28. Weber, G. Biochemical strategy of cancer cells and the design of chemotherapy: G. H. A. Clowes Memorial Lecture. *Cancer Res.* **1983**, *43*, 3466–3492.
29. Hedstrom, L.; Liechti, G.; Goldberg, J.B.; Gollapalli, D.R. The antibiotic potential of prokaryotic IMP dehydrogenase inhibitors. *Curr. Med. Chem.* **2011**, *18*, 1909–1918. [[CrossRef](#)]
30. Usha, V.; Hobrath, J.V.; Gurucha, S.S.; Reynolds, R.C.; Besra, G.S. Identification of novel Mt-Guab2 inhibitor series active against *M. tuberculosis*. *PLoS ONE* **2012**, *7*, e33886. [[CrossRef](#)]
31. Rao, V.A.; Shepherd, S.M.; Owen, R.; Hunter, W.N. Structure of *Pseudomonas aeruginosa* inosine 5'-monophosphate dehydrogenase. *Acta Crystallograph. Sect. F Struct. Biol. Cryst. Commun.* **2013**, *69*, 243–247. [[CrossRef](#)] [[PubMed](#)]
32. Mandapati, K.; Gorla, S.K.; House, A.L.; McKenney, E.S.; Zhang, M.; Rao, S.N.; Gollapalli, D.R.; Mann, B.J.; Goldberg, J.B.; Cuny, G.D.; et al. Repurposing cryptosporidium inosine 5'-monophosphate dehydrogenase inhibitors as potential antibacterial agents. *ACS Med. Chem. Lett.* **2014**, *5*, 846–850. [[CrossRef](#)]
33. Prosise, G.L.; Luecke, H. Crystal structures of *Trichomonas foetus* inosine monophosphate dehydrogenase in complex with substrate, cofactor and analogs: A structural basis for the random-in ordered-out kinetic mechanism. *J. Mol. Biol.* **2003**, *326*, 517–527. [[CrossRef](#)]
34. Makowska-Grzyska, M.; Kim, Y.; Wu, R.; Wilton, R.; Gollapalli, D.R.; Wang, X.K.; Zhang, R.; Jedrzejczak, R.; Mack, J.C.; Maltseva, N.; et al. *Bacillus anthracis* inosine 5'-monophosphate dehydrogenase in action: The first bacterial series of structures of phosphate ion-, substrate-, and product-bound complexes. *Biochemistry* **2012**, *51*, 6148–6163. [[CrossRef](#)] [[PubMed](#)]
35. Labesse, G.; Alexandre, T.; Gelin, M.; Haouz, A.; Munier-Lehmann, H. Crystallographic studies of two variants of *Pseudomonas aeruginosa* IMPDH with impaired allosteric regulation. *Acta Crystallograph. Sect. D Biol. Crystallograph.* **2015**, *71*, 1890–1899. [[CrossRef](#)] [[PubMed](#)]
36. Hedstrom, L. IMP dehydrogenase: Structure, mechanism, and inhibition. *Chem. Rev.* **2009**, *109*, 2903–2928. [[CrossRef](#)]
37. Nimmegern, E.; Black, J.; Futer, O.; Fulghum, J.R.; Chambers, S.P.; Brummel, C.L.; Raybuck, S.A.; Sintchak, M.D. Biochemical analysis of the modular enzyme inosine 5'-monophosphate dehydrogenase. *Protein Expr. Purif.* **1999**, *17*, 282–289. [[CrossRef](#)]

38. Pimkin, M.; Markham, G.D. The CBS subdomain of inosine 5'-monophosphate dehydrogenase regulates purine nucleotide turnover. *Mol. Microbiol.* **2008**, *68*, 342–359. [[CrossRef](#)]
39. Makowska-Grzyska, M.; Kim, Y.; Maltseva, N.; Osipiuk, J.; Gu, M.; Zhang, M.; Mandapati, K.; Gollapalli, D.R.; Gorla, S.K.; Hedstrom, L.; et al. A novel cofactor-binding mode in bacterial IMP dehydrogenases explains inhibitor selectivity. *J. Biol. Chem.* **2015**, *290*, 5893–5911. [[CrossRef](#)]
40. Gollapalli, D.R.; Macpherson, I.S.; Liechti, G.; Gorla, S.K.; Goldberg, J.B.; Hedstrom, L. Structural determinants of inhibitor selectivity in prokaryotic IMP dehydrogenases. *Chem. Biol.* **2010**, *17*, 1084–1091. [[CrossRef](#)]
41. Chen, L.; Wilson, D.J.; Xu, Y.; Aldrich, C.C.; Felczak, K.; Sham, Y.Y.; Pankiewicz, K.W. Triazole-linked inhibitors of inosine monophosphate dehydrogenase from human and *Mycobacterium tuberculosis*. *J. Med. Chem.* **2010**, *53*, 4768–4778. [[CrossRef](#)] [[PubMed](#)]
42. Umejiego, N.N.; Gollapalli, D.; Sharling, L.; Volftsun, A.; Lu, J.; Benjamin, N.N.; Stroupe, A.H.; Riera, T.V.; Striepen, B.; Hedstrom, L. Targeting a prokaryotic protein in a eukaryotic pathogen: Identification of lead compounds against cryptosporidiosis. *Chem. Biol.* **2008**, *15*, 70–77. [[CrossRef](#)] [[PubMed](#)]
43. Kirubakaran, S.; Gorla, S.K.; Sharling, L.; Zhang, M.; Liu, X.; Ray, S.S.; Macpherson, I.S.; Striepen, B.; Hedstrom, L.; Cuny, G.D. Structure-activity relationship study of selective benzimidazole-based inhibitors of *Cryptosporidium parvum* IMPDH. *Bioorg. Med. Chem. Lett.* **2012**, *22*, 1985–1988. [[CrossRef](#)] [[PubMed](#)]
44. Gorla, S.K.; Kavitha, M.; Zhang, M.; Chin, J.E.W.; Liu, X.; Striepen, B.; Makowska-Grzyska, M.; Kim, Y.; Joachimiak, A.; Hedstrom, L.; et al. Optimization of benzoxazole-based inhibitors of *Cryptosporidium parvum* inosine 5'-monophosphate dehydrogenase. *J. Med. Chem.* **2013**, *56*, 4028–4043. [[CrossRef](#)] [[PubMed](#)]
45. Gorla, S.K.; Zhang, Y.; Rabideau, M.M.; Qin, A.; Chacko, S.; House, A.L.; Johnson, C.R.; Mandapati, K.; Bernstein, H.M.; McKenney, E.S.; et al. Benzoxazoles, Phthalazinones, and Arylurea-Based Compounds with IMP Dehydrogenase-Independent Antibacterial Activity against *Francisella tularensis*. *Antimicrob. Agents Chemother.* **2017**, *61*, e00939-17. [[CrossRef](#)]
46. Chacko, S.; Boshoff, H.I.M.; Singh, V.; Ferraris, D.M.; Gollapalli, D.R.; Zhang, M.; Lawson, A.P.; Pepi, M.J.; Joachimiak, A.; Rizzi, M.; et al. Expanding Benzoxazole-Based Inosine 5'-Monophosphate Dehydrogenase (IMPDH) Inhibitor Structure-Activity As Potential Antituberculosis Agents. *J. Med. Chem.* **2018**, *61*, 4739–4756. [[CrossRef](#)]
47. Park, Y.; Pacitto, A.; Bayliss, T.; Cleghorn, L.A.T.; Wang, Z.; Hartman, T.; Arora, K.; Ioerger, T.R.; Sacchetti, J.; Rizzi, M.; et al. Essential but Not Vulnerable: Indazole Sulfonamides Targeting Inosine Monophosphate Dehydrogenase as Potential Leads against *Mycobacterium tuberculosis*. *ACS Infect. Dis.* **2017**, *3*, 18–33. [[CrossRef](#)]
48. Maurya, S.K.; Gollapalli, D.R.; Kirubakaran, S.; Zhang, M.; Johnson, C.R.; Benjamin, N.N.; Hedstrom, L.; Cuny, G.D. Triazole inhibitors of *Cryptosporidium parvum* inosine 5'-monophosphate dehydrogenase. *J. Med. Chem.* **2009**, *52*, 4623–4630. [[CrossRef](#)]
49. Sahu, N.U.; Singh, V.; Ferraris, D.M.; Rizzi, M.; Kharkar, P.S. Hit discovery of *Mycobacterium tuberculosis* inosine 5'-monophosphate dehydrogenase, GuaB2, inhibitors. *Bioorg. Med. Chem. Lett.* **2018**, *28*, 1714–1718. [[CrossRef](#)]
50. Sahu, N.U.; Purushothaman, G.; Thiruvengatam, V.; Kharkar, P.S. Design, synthesis, and biological evaluation of *Helicobacter pylori* inosine 5'-monophosphate dehydrogenase (HpIMPDH) inhibitors. *Drug Dev. Res.* **2019**, *80*, 125–132. [[CrossRef](#)]
51. Makowska-Grzyska, M.; Kim, Y.; Gorla, S.K.; Wei, Y.; Mandapati, K.; Zhang, M.; Maltseva, N.; Modi, G.; Boshoff, H.I.; Gu, M.; et al. *Mycobacterium tuberculosis* IMPDH in Complexes with Substrates, Products and Antitubercular Compounds. *PLoS ONE* **2015**, *10*, e0138976. [[CrossRef](#)] [[PubMed](#)]
52. Usha, V.; Gurucha, S.S.; Lovering, A.L.; Lloyd, A.J.; Papaemmanouil, A.; Reynolds, R.C.; Besra, G.S. Identification of novel diphenyl urea inhibitors of Mt-GuaB2 active against *Mycobacterium tuberculosis*. *Microbiology* **2011**, *157*, 290–299. [[CrossRef](#)] [[PubMed](#)]
53. Gorla, S.K.; Kavitha, M.; Zhang, M.; Liu, X.; Sharling, L.; Gollapalli, D.R.; Striepen, B.; Hedstrom, L.; Cuny, G.D. Selective and potent urea inhibitors of *Cryptosporidium parvum* inosine 5'-monophosphate dehydrogenase. *J. Med. Chem.* **2012**, *55*, 7759–7771. [[CrossRef](#)] [[PubMed](#)]
54. Beevers, R.E.; Buckley, G.M.; Davies, N.; Fraser, J.L.; Galvin, F.C.; Hannah, D.R.; Haughan, A.F.; Jenkins, K.; Mack, S.R.; Pitt, W.R.; et al. Low molecular weight indole fragments as IMPDH inhibitors. *Bioorg. Med. Chem. Lett.* **2006**, *16*, 2535–2538. [[CrossRef](#)]

55. Beevers, R.E.; Buckley, G.M.; Davies, N.; Fraser, J.L.; Galvin, F.C.; Hannah, D.R.; Haughan, A.F.; Jenkins, K.; Mack, S.R.; Pitt, W.R.; et al. Novel indole inhibitors of IMPDH from fragments: Synthesis and initial structure-activity relationships. *Bioorg. Med. Chem. Lett.* **2006**, *16*, 2539–2542. [[CrossRef](#)]
56. Watterson, S.H.; Carlsen, M.; Dhar, T.G.M.; Shen, Z.; Pitts, W.J.; Guo, J.; Gu, H.H.; Norris, D.; Chorba, J.; Chen, P.; et al. Novel inhibitors of IMPDH: A highly potent and selective quinolone-based series. *Bioorg. Med. Chem. Lett.* **2003**, *13*, 543–546. [[CrossRef](#)]
57. Jangra, S.; Purushothaman, G.; Juvale, K.; Ravi, S.; Menon, A.; Thiruvenkatam, V.; Kirubakaran, S. Synthesis and In Vitro Enzymatic Studies of New 3-Aryldiazanyl Indoles as Promising *Helicobacter pylori* IMPDH Inhibitors. *Curr. Top. Med. Chem.* **2019**, *19*, 376–382. [[CrossRef](#)]
58. Nystroem, K.; Waldenstroem, J.; Tang, K.-W.; Lagging, M. Ribavirin: Pharmacology, multiple modes of action and possible future perspectives. *Future Virol.* **2019**, *14*, 153–160. [[CrossRef](#)]
59. Ishikawa, H. Mizoribine and mycophenolate mofetil. *Curr. Med. Chem.* **1999**, *6*, 575–597. [[PubMed](#)]
60. Cao, S.; Aboge, G.O.; Terkawi, M.A.; Zhou, M.; Kamyngkird, K.; Moumouni, P.F.A.; Masatani, T.; Igarashi, I.; Nishikawa, Y.; Suzuki, H.; et al. Mycophenolic acid, mycophenolate mofetil, mizoribine, ribavirin, and 7-nitroindole inhibit propagation of Babesia parasites by targeting inosine 5'-monophosphate dehydrogenase. *J. Parasitol.* **2014**, *100*, 522–526. [[CrossRef](#)]
61. Sarwono, A.E.Y.; Mitsunashi, S.; Kabir, M.H.B.; Shigetomi, K.; Okada, T.; Ohsaka, F.; Otsuguro, S.; Maenaka, K.; Igarashi, M.; Kato, K.; et al. Repurposing existing drugs: Identification of irreversible IMPDH inhibitors by high-throughput screening. *J. Enzyme Inhib. Med. Chem.* **2019**, *34*, 171–178. [[CrossRef](#)] [[PubMed](#)]
62. Juvale, K.; Shaik, A.; Kirubakaran, S. Inhibitors of inosine 5'-monophosphate dehydrogenase as emerging new generation antimicrobial agents. *MedChemComm* **2019**, *10*, 1290–1301. [[CrossRef](#)] [[PubMed](#)]
63. Juvale, K.; Purushothaman, G.; Singh, V.; Shaik, A.; Ravi, S.; Thiruvenkatam, V.; Kirubakaran, S. Identification of selective inhibitors of *Helicobacter pylori* IMPDH as a targeted therapy for the infection. *Sci. Rep.* **2019**, *9*, 190. [[CrossRef](#)] [[PubMed](#)]
64. Yang, N.; Wang, J.; Li, J.; Wang, Q.-H.; Wang, Y.; Cheng, M.-S. A three-dimensional pharmacophore model for IMPDH inhibitors. *Chem. Biol. Drug Des.* **2011**, *78*, 175–182. [[CrossRef](#)]
65. Freedman, R.; Yu, R.; Sarkis, A.W.; Hedstrom, L. A structural determinant of mycophenolic acid resistance in eukaryotic inosine 5'-monophosphate dehydrogenases. *Protein Sci. Publ. Protein Soc.* **2020**, *29*, 686–694. [[CrossRef](#)]
66. Sun, X.E.; Hansen, B.G.; Hedstrom, L. Kinetically controlled drug resistance: How *Penicillium brevicompactum* survives mycophenolic acid. *J. Biol. Chem.* **2011**, *286*, 40595–40600. [[CrossRef](#)]
67. Minor, W.; Cymborowski, M.; Otwinowski, Z.; Chruszcz, M. HKL-3000: The integration of data reduction and structure solution—From diffraction images to an initial model in minutes. *Acta Crystallograph. Sect. D Biol. Crystallograph.* **2006**, *62*, 859–866. [[CrossRef](#)]
68. Adams, P.D.; Afonine, P.V.; Bunkóczi, G.; Chen, V.B.; Davis, I.W.; Echols, N.; Headd, J.J.; Hung, L.-W.; Kapral, G.J.; Grosse-Kunstleve, R.W.; et al. PHENIX: A comprehensive Python-based system for macromolecular structure solution. *Acta Crystallograph. Sect. D Biol. Crystallograph.* **2010**, *66*, 213–221. [[CrossRef](#)]
69. Fiser, A.; Do, R.K.; Sali, A. Modeling of loops in protein structures. *Protein Sci.* **2000**, *9*, 1753–1773. [[CrossRef](#)]
70. Laskowski, R.A.; Macarthur, M.W.; Moss, D.S.; Thornton, J.M. Procheck—A Program to Check the Stereochemical Quality of Protein Structures. *J. Appl. Crystallograph.* **1993**, *26*, 283–291. [[CrossRef](#)]
71. Eisenberg, D.; Luthy, R.; Bowie, J.U. VERIFY3D: Assessment of protein models with three-dimensional profiles. *Methods Enzymol.* **1997**, *277*, 396–404. [[PubMed](#)]
72. Wu, G.; Robertson, D.H.; Brooks, C.L.; Vieth, M. Detailed analysis of grid-based molecular docking: A case study of CDOCKER-A CHARMM-based MD docking algorithm. *J. Comput. Chem.* **2003**, *24*, 1549–1562. [[CrossRef](#)] [[PubMed](#)]
73. Kerr, K.M.; Digits, J.A.; Kuperwasser, N.; Hedstrom, L. Asp338 controls hydride transfer in *Escherichia coli* IMP dehydrogenase. *Biochemistry* **2000**, *39*, 9804–9810. [[CrossRef](#)] [[PubMed](#)]

Sample Availability: Samples of the compounds are not available from the authors.



© 2020 by the authors. Licensee MDPI, Basel, Switzerland. This article is an open access article distributed under the terms and conditions of the Creative Commons Attribution (CC BY) license (<http://creativecommons.org/licenses/by/4.0/>).